Title: CFD modelling of Expanded Metal Porous Matrix Heat Exchangers for Intensified Carbon Capture Applications.

Authors: James Hendry*[1]; David Reay[1]; Jonathan Lee[1]

***corresponding author.** Tel.: +44 1912085747. E-mail address: james.hendry@newcastle.ac.uk

Affiliation: [1] School of Engineering, Merz Court, Newcastle University. Newcastle upon Tyne, NE1 7RU, UK.

Abstract: Expanded Metal Porous Matrix Heat Exchangers (EM-PMHE) use a fin structure based on stacked sheets of expanded metal. This fin structure creates a three-dimensional flow that also enhances heat transfer. EM-PMHEs are of interest in applications for amine-based carbon-capture processes. Their compact design could intensify heat exchange processes in the amine absorption cycle. The transport properties of EM-PMHEs are also of interest for applications in rotating packed beds, where expanded metal can make an effective packing material. This work examines a EM-PMHE using computational fluid dynamics. The heat transfer prediction of the model is validated against experimental data from literature. A simple 1D model is also presented for comparison. The model is used to evaluate the potential of EM-PMHEs in amine-based carbon-capture applications, Demonstrating a potential order-of-magnitude reduction in equipment size of amine capture processes using EM-PMHEs.

Keywords: expanded metal; porous matrix heat exchanger; process intensification; compact heat exchanger.

Highlights:

- A computational fluid dynamics model of heat exchange in an expanded metal porous matrix heat exchanger is presented.
- Results are validated against experimental data from literature.
- A 1-dimensional heat transfer model is also presented and compared to experiment and simulation.
- The performance is evaluated as a compact heat exchanger for amine-based carbon capture applications.

Nomenclature

,α	,CO_2 loading (dissolved CO_2 in the amine solution)	$^{mol\ CO2}/_{mol\ MEA}$
,C_p	,specific heat capacity	W/kgK
,d_h	hydraulic diameter	,m
,f	Fanning friction factor	
,G	,gas flowrate	,kg/s
,h	,heat transfer coefficient	W/m^2K
,ΔH_r	,heat-of-reaction	J/kg
,j	Chilton-Colburn j-factor	
,L	,length	,m
,$\dot{m}$	,massflow	,kg/s
,ΔP	,pressure drop	,Pa
,u	velocity (average)	,m/s
,ρ	density,	,kg/m^3
,ω	,rotation speed	,rad/s
,μ	,dynamic viscosity	,Pa.s
Nu	Nusselt Number from hydraulic diameter	
Re	Reynold's number from hydraulic diameter	
St	Stanton Number	
Pr	Prandtl Number	

Abbreviations

CCS: carbon capture and storage.

CFD: computational fluid dynamics.

CSA: cross-sectional area

EM-PMHE: Expanded metal porous matrix heat exchanger. A type of plate-fin heat exchanger developed by Hesselgreaves, where fins are made from stacked layers of expanded metal sheet.

RPB: rotating packed beds.

Transition-SST: transition shear stress transport, turbulence model in CFD.

1. Introduction

Carbon-capture is becoming a reality for many process industry sectors. In the UK, government commitments to achieve net-zero greenhouse gas emissions by 2050, require emissions from process industries of 40 $MtCO_2$/a (UKRI, 2021) to be reduced to zero. Carbon capture from process industry clusters will play a significant role in this. Several full-scale CCS demonstrations of this kind are planned for the near-future, including Zero-carbon Humber (UK) (Zero Carbon Humber, 2021), Gassnova (Norway) (Doyle, 2020), and Porthos (Netherlands) (Porthos Development C.V., 2021) projects. Amine-based carbon-capture is the most established carbon-capture technology, and it will be vital to future CCS infrastructures. The drawbacks of amine-based carbon capture could be addressed through process intensification.

Rotating packed beds (RPBs) can be used to intensify amine-based carbon-capture processes. RPBs replace gravity flow in conventional absorption columns with centrifugal forces under rotation. This reduces equipment sizes substantially. Newcastle University has a long history of research in this area (1) (2) (3). Initial mass transfer studies (4), revealed that expanded metal sheets were an efficient packing material for RPBs. Expanded metal packing was later used for performance benchmarking in the RPB CCS pilot-plant at Newcastle University. Several properties made it effective as a packing for benchmarking: the packing characteristics (surface area, voidage) are well-defined and comparable to commercial packings, whilst being of a non-proprietary design. The material (stainless steel) is corrosion-resistant and low-cost when compared to alternative RPB packings often used in research, such as nickel-metal foams. For this reason, the mass, momentum, and heat transfer for fluid flows inside expanded metal packings is of interest to RPB research. This has been studied both experimentally (5) and through CFD (6). Though the heat transfer properties in expanded metal RPB packings remain relatively unexplored, they are however very important. Due to the enthalpy of reaction, the reactive absorption process inside the RPB creates temperature changes that affect the mass transfer process. This is one motivation for the present research.

A process intensification design philosophy can be applied to individual plant equipment in this way: replacing conventional columns with RPBs. However, process intensification is most effective when applied to the process as a holistic whole. Amine-based carbon-capture processes use several heat exchangers. These are vitally important to economics of carbon-capture process. The lean/rich heat exchanger makes up ca. 37% of total plant capital costs (7), while reboiler duties dominate operational costs. The size of these heat exchangers increases proportionally during scale-up. For full-scale processes, these heat exchangers can become major plant equipment in-of-themselves. A recent case-study sized to treat flue gas from the Norcem Heidelberg, cement plant in Brevik (130,000Nm3/hr 22% CO_2) predicted a required heat exchange surface of 21200 m^2 for the lean/rich heat exchanger alone, using conventional technology (shell-and-tube) (7). Previously, the present authors (8) have suggested printed circuit heat exchangers to replace conventional technology for lean/rich heat exchange. Expanded metal porous matrix heat exchangers (EM-PMHEs) could provide an equivalent benefit whilst being easier to manufacture. This work will explore the potential of EM-PMHEs in amine-based carbon-capture. A model of an EM-PMHE is validated using experimental data from literature (9). The model is then applied to determine heat transfer coefficients in monoethanolamine solutions. This data will be used to compare to conventional heat exchanger designs in carbon-capture processes.

1.1 Description of EM-PMHE

The porous matrix heat exchanger was originally developed by Hesselgreaves (10). They consist of a plate-fin heat exchanger construction. Fins are assembled from stacked layers of a perforated sheet metal, with expanded metal being the most common choice. Layers of expanded metal are stacked in an offset, alternating pattern. The layers of material overlap at the same location between the adjacent layers. The layers are then bonded together. This creates a contact area between the expanded metal layers, that can conduct heat (see conducting column (d), in Figure 1, below).

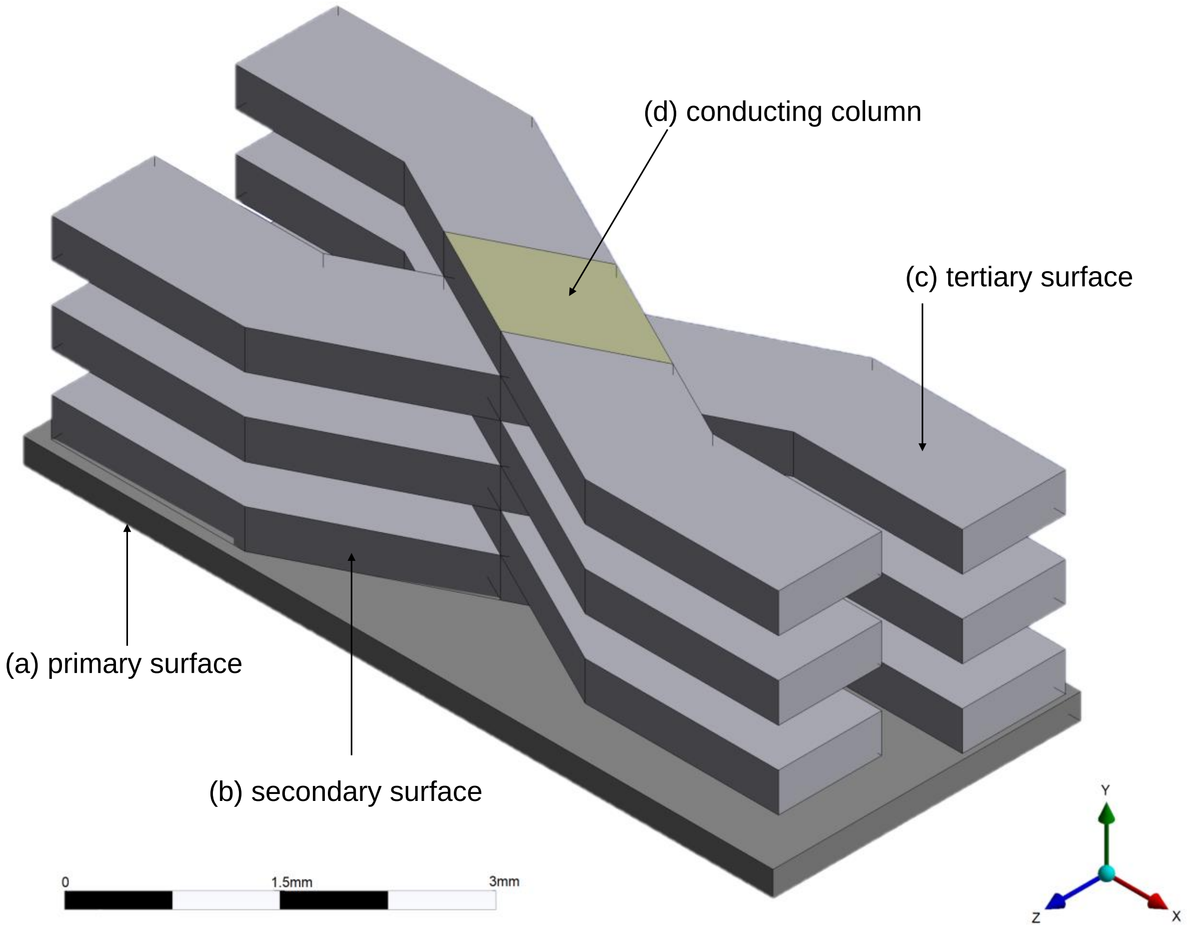

Figure 1: Section sketch illustrating construction of porous matrix heat exchanger.

The overall construction is shown in Figure 1. The primary surface (a) is the flat plate surface of the heat exchanger, separating the two fluids. The secondary surface (b) is the first layer of expanded metal. This conducts more heat than the layers above, because the entire bottom surface of the secondary surface (b) in direct contact with the primary surface (a). The conducting column (d) is made up of the contact surfaces between layers, and serves as the main fin structure, conducting heat in the Y-direction. The tertiary surface (c) branches off of the conducting column, providing an extended surface for heat transfer, serving as an additional fin structure. The structure of the EM-PMHE creates 3D flow patterns: the tertiary surface (c) also acts as a turbulence promoter enhancing heat transfer.

1.2 EM-PMHE, Applications to amine duties

To-date, EM-PMHEs have some applications industrially. Chart Industries Inc. have applied the design to compact heat exchangers and micro-reactor units. Absotech GmbH also investigated them for intensified ammonia absorption chillers (11). More recently, EM-PMHEs have been investigated for applications in phase-change materials, the fin structure acting as a composite metallic matrix (12) . EM-PMHEs could have benefits in amine duties. Amine solutions are corrosive and often require stainless steel construction. This increases manufacturing costs, particularly for full-scale units. Stainless steel also has a lower thermal conductivity, 19.64 W/mK (vs. 100W/mK for carbon steel, 280W/mK for aluminium, 400W/mK for copper (13)) when compared to other metals. This places a limit on the fin efficiency for stainless steel constructions. This is particularly important for fin efficiency in intensified equipment, where high heat transfer coefficients also make fins less effective. The thick fin cross section of the tertiary surfaces of the EM-PMHE are expected to aid in this respect. The viscosity of amine solutions can increase substantially depending on solution concentrations, temperature and CO_2 loadings. The flow enhancement and the high surface area of the EM-PMHE is expected to provide a benefit in this regard.

2 Geometry

The domain geometry used in the simulation is based on the description given by Hesselgreaves (9) for the "M2a" test-piece. Data was also obtained from the following sources: dimensions extracted from photographs in the original source (9); data from the equipment suppliers (14); measurements of comparable material samples, taken in the laboratory. These sources were found to agree to within 0.5 mm with the dimensions shown in Figure 2, and any discrepancies between the are likely due to manufacturing tolerances for the expanded metal.

A sketch of the test-piece from (9) is shown in Figure 3. The experimental test-piece consisted of a plate-fin heat exchanger, contacting a hot airflow with cooling water at ambient temperature. 8 air-side plates contained the EM-PMHE fin construction, while 9 water-side plates provided cooling. The EM-PMHE is assembled from six layers of expanded metal sheet (Expamet 198C. (14)) of 0.381mm thickness (air-side plate spacing = 2.28mm). The test-piece was installed in a 50x50mm square duct and was 33mm in length. Little detail is given in the original source regarding the water-side flow. Given that the water-side thermal resistance is low (9) and no increase (<1ºC) in water temperature was observed during the experiment, it is appropriate to model the water-side as a constant temperature surface.

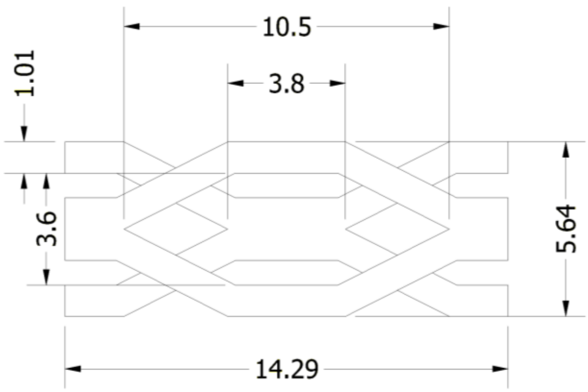

Figure 2: dimensions of expanded metal in model. Showing two expanded metal layers.

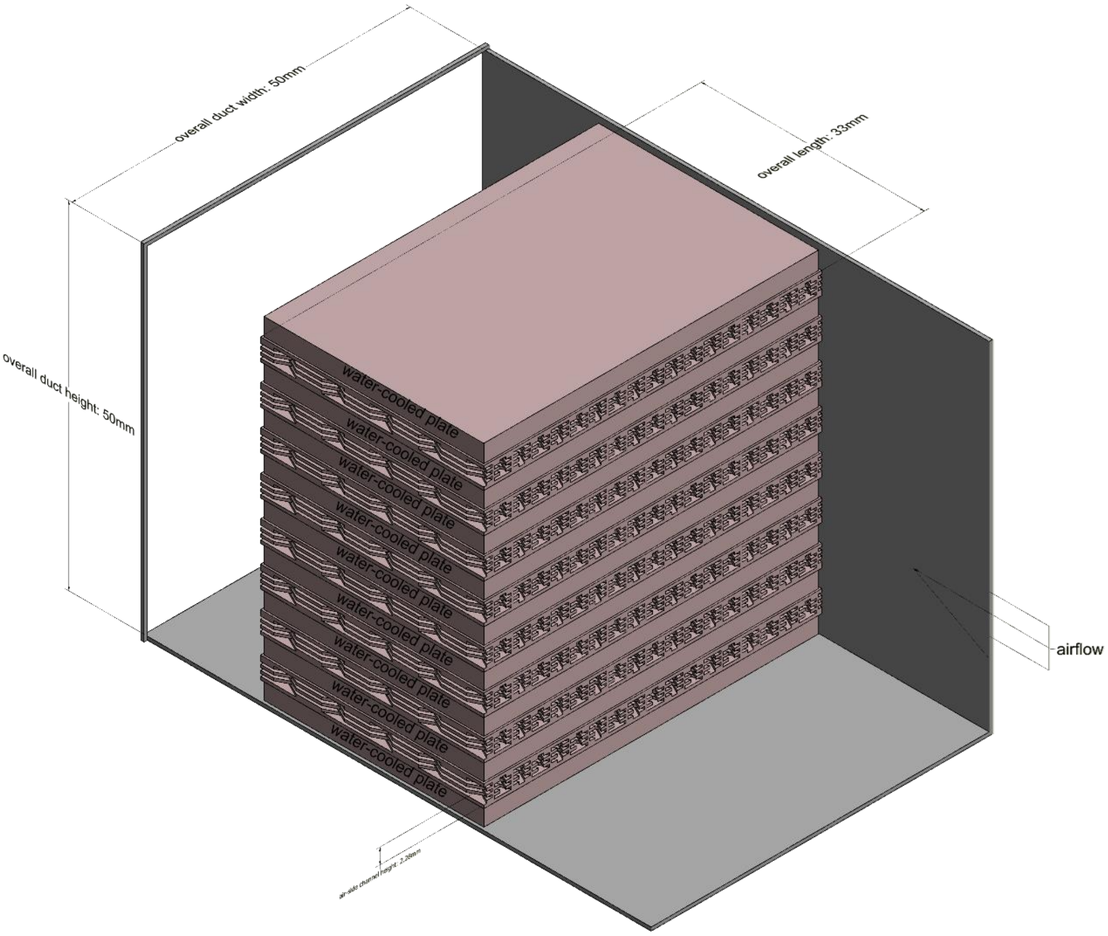

Figure 3: sketch of M2a test-piece inside duct (9).

2.1 CFD model geometry and boundary conditions

The geometry used for CFD modelling represents a symmetrical section through one row of the conducting columns, visible in Figure 3. Symmetry planes were used to reduce computational load. Walls were defined at the top and base of the model to represent the primary surfaces, and conduct heat out of the domain. A constant-velocity inlet (from

Table 1) and constant-pressure outlet (1atm.) defined the flow conditions (red in Figure 4). Buoyancy effects can be neglected, as natural convection is negligible (Richardson number = 0.0001 at lowest flowrate).

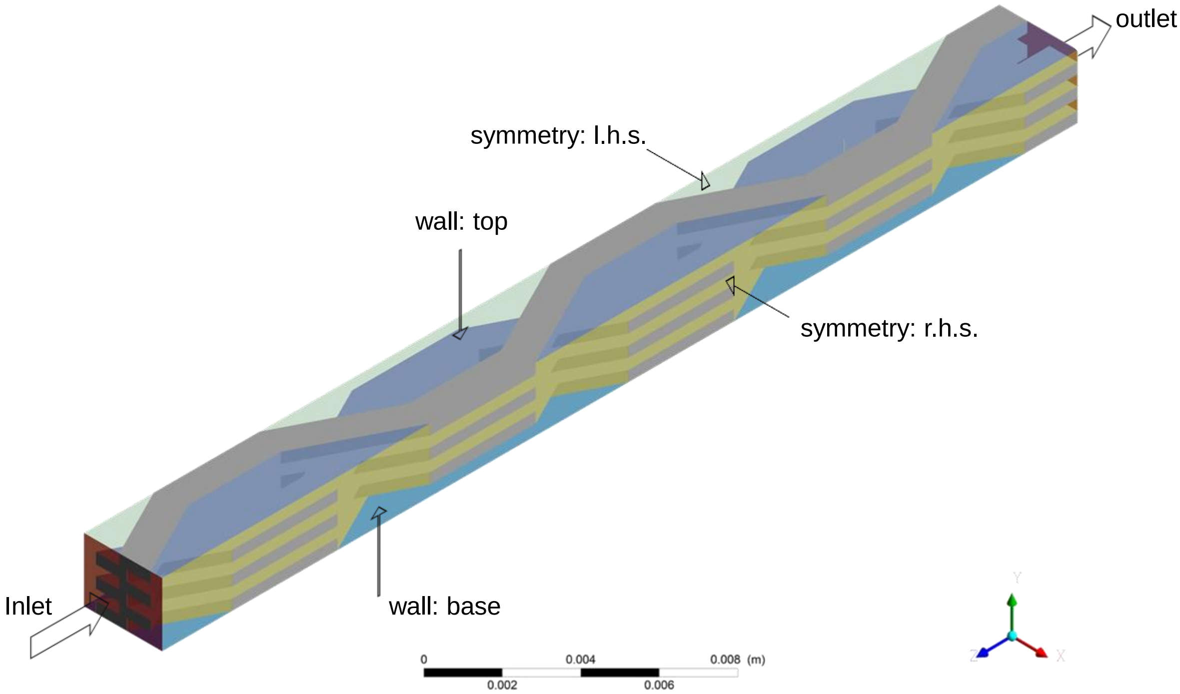

Figure 4 CFD Model geometry

3 Experimental data

Experimental data was extracted from the source material (9) using a plot digitiser (15). Data on pressure drop and heat transfer is presented in dimensionless form, as friction factor, and j-factor respectively, vs. Reynolds number. To interpret these results, the present authors used the definitions presented in Hesselgreaves (16), respectively:

Equation 1: Reynold's number, where d_h = hydraulic diameter, 1.362mm

$$Re = \frac{\rho u d_h}{\mu}$$

Equation 2: fanning friction factor, for pressure drop data.

$$\Delta P = \frac{1}{2}\rho u^2 \frac{4L}{d_h} f$$

Equation 3: Colburn j-factor, for heat transfer coefficient h..

$$j = St.Pr^{\frac{2}{3}} \quad where \quad St = \frac{h}{\rho u C_p}$$

Table 1: experimental results for fanning friction factor and Colburn j-factor vs. Reynold's number. Showing their interpretation using properties of air at 25°C.

Re	f	j	u (m/s)	ΔP (Pa)	h (W/m²K)
Reynold's no	Fanning friction factor	Colburn j-factor	velocity, inside HX	pressure drop	heat transfer coefficient
500	0.23	0.037	5.7	430	310
577	0.21	0.035	6.6	533	341
651	0.20	0.032	7.4	640	358
779	0.19	0.029	8.9	867	386
914	0.18	0.028	10.4	1110	428
1046	0.17	0.025	11.9	1353	452
1231	0.16	0.024	14.0	1837	499
1373	0.15	0.023	15.6	2092	526
1586	0.14	0.021	18.1	2637	563
1966	0.13	0.019	22.4	3801	631
2417	0.12	0.017	27.5	5319	710
3081	0.12	0.015	35.1	8269	808
4003	0.11	0.014	45.6	13355	946
4989	0.11	0.013	56.8	19767	1087

4. Grid Independence

Early simulations predicted that flow is transitional at the lowest Reynolds numbers in the experiment. Grid independence was established with a flow-only model using two successive grid doublings. An inlet velocity was chosen (27.5m/s, Re = 2400) to represent conditions over the experimental range. The result is given in Table 2.

Table 2: grid independence

	coarse	Medium	Fine
Cell count	500,000	3,000,000	30,000,000
Cells a/c 0.381mm gap	4	8	16
,y+	7.7	3.9	1.9
ΔP (Pa)	3958	4504	4577

Mesh quality was assessed against the skewness mesh quality metric. Acceptance criteria for convergence were based on (17) (18). Criterion of <0.9 maximum skewness and <0.3 average skewness were used to determine an acceptable mesh. Iterative convergence was achieved to below $1x10^{-4}$ residuals. Fully second-order discretisation was applied to all transport variables.

5. one-dimensional model

A simple one-dimensional model of the geometry was also prepared, based on a sum-of-resistances approach. Symmetrical fin surfaces that are equally cooled from a sink on both sides have no net heat conduction across the plane of symmetry. For 1D fin models symmetrical surfaces behave as insulated boundaries. In this case, for the 1D model, the geometry shown in Figure 1 can be further simplified, to model 3 layers of expanded metal. A 1D model of the geometry shown in Figure 4 is described in Table 3. This model approximates the expanded metal layers (the secondary surface and tertiary surfaces in Figure 1) as rectangular fins. The secondary surfaces are modelled as fins with convective tips, as a substantial amount of heat transfer will flow vertically through this fin from the fin tip into the plate. The tertiary surfaces are modelled as rectangular fins with insulated tips. The perimeter and cross section of the fin were calculated based on the layer thickness = 0.381mm, and strand width = 1.01mm. The effective length of the fin L_7 =2.9mm in the model was then chosen to match the total area of the fin in contact with the fluid. The remaining heat transfer surfaces in contact with the fluid were modelled as simple plate conduction. The heat transfer coefficient was obtained using the Gnielinski correlation with transition flow correction (19).

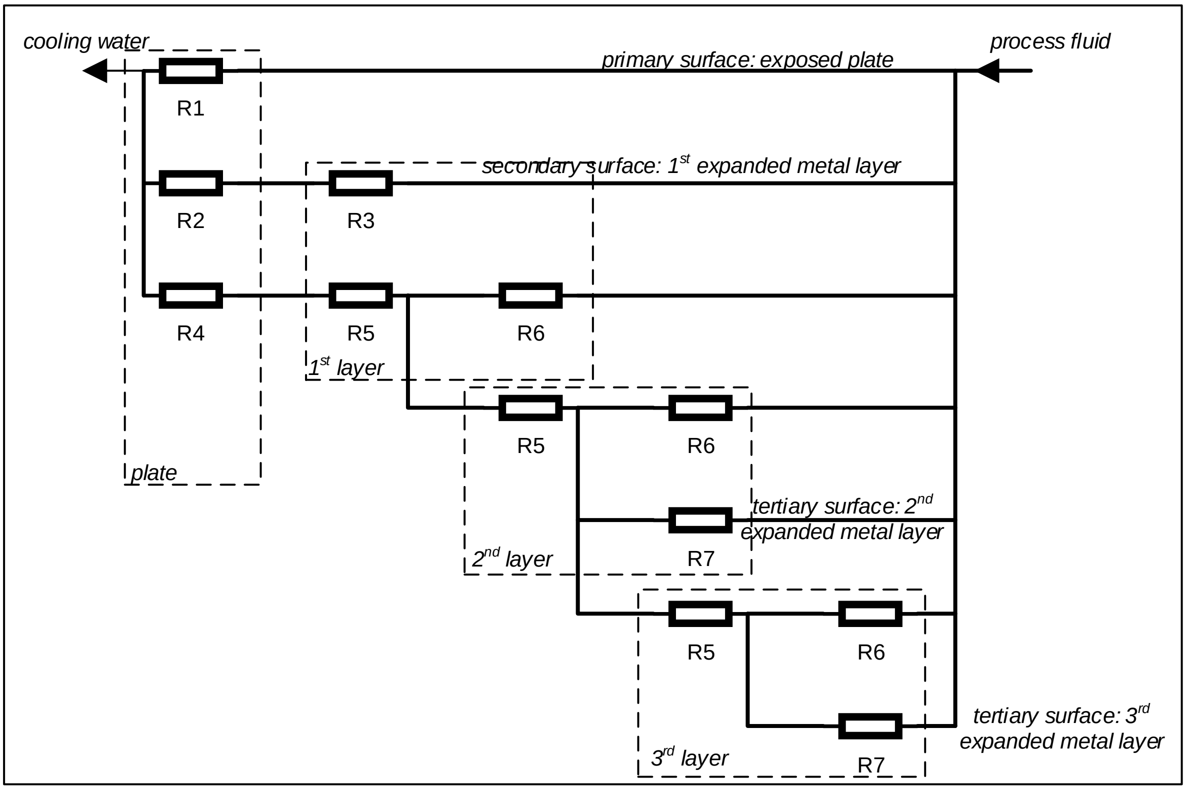

Figure 5 1D model illustration.

Table 3: 1D model

Name	description	formula	inputs
R1	exposed plate surface (primary surface)	$R_1 = \frac{1}{hA_1} + \frac{L_1}{kA_1}$	A_1 = 5.76x10^{-5} m^2 L_1 = 0.45 mm
R2	bonded plate surface, excluding conducting column	$R_2 = \frac{L_1}{kA_2}$	A_2 = 2.88x10^{-5} m^2
R3	first expamet layer (secondary surface)	Consider as a fin with tip convection $R_3 = \frac{1}{\sqrt{hP_3kA_{c3}}} \cdot \frac{\cosh(m_3L_3) + \left(h/_{m_3k}\right)\sinh(m_3L_3)}{\sinh(m_3L_3) + \left(h/_{m_3k}\right)\cosh(m_3L_3)}$ $m_3 = \sqrt{\frac{hP_3}{kA_{c3}}}$	A_{c3} = 3.20x10^{-6} m^2 Cross-sectional area of one fin. P_3 = 4.4mm Perimeter in contact with fluid. L_3 = 0.381 mm Height of expanded metal layer ,x nine fins.
R4	bonded plate surface, under conducting column	$R_4 = \frac{L_1}{kA_4}$	A_4 = 1.28x10^{-6} m^2, Cross-sectional area of conducting column
R5	Conduction through one layer of conducting column	$R_5 = \frac{L_3}{kA_4}$	
R6	Convection on exposed surface of conducting column	$R_6 = \frac{1}{hA_6}$	A_6 = 4.8x$10^{-7}$$m^2$,x two surfaces, per layer
R7	Second/third expamet layer (tertiary surface)	Consider as rectangular fin with insulated tip $R_7 = \frac{1}{\sqrt{hP_7kA_{c7}}} \frac{1}{\tanh(mL_7)}$ $m_3 = \sqrt{\frac{hP_7}{kA_{c7}}}$	A_{c7} = 3.89x$10^{-7}$$m^2$ P_7 = 2.79 mm L_7 = 2.90 mm ,x two per layer, x1 for inlet conducting column.
R4,R5, R6,R7	Represent model of one conducting column plus tertiary surfaces	*Addition of resistances R4,R5,R6,R7 for each conducting column and it's tertiary surfaces. Then added together in parallel to represent the 5 conducting columns in the geometry.*	

6. Validation

The validation results are shown below in Figure 6. Figure 6 (i) shows the pressure drop prediction versus experiment. A substantial portion of the pressure drop is due to losses in sudden expansion and contraction at the entrance and exit of the test piece. The solid line in Figure 6 (i) shows the result from the CFD model with the addition of loss terms for sudden expansion and contraction (20). Figure 6(ii) shows the heat transfer result obtained based on the inlet and outlet temperatures and using the log-mean temperature method. This validates that the simulation predicts the experimental result within the uncertainty of the experimental data. It also demonstrates that the turbulence model choice is appropriate for the simulation. The result from the Gnielinski correlation is also shown in the purple dotted line in Figure 6(ii). This shows good comparison to the 3D CFD result. The plot in Figure 6 (iii) shows the transition flow characteristics in regions between the two layers. This demonstrates that the chosen turbulence model – Transition SST model (21) - agrees with both laminar and turbulent (k-e) results indicating that it is valid of the transition range. The transition SST model uses additional transport variables to model transition flow using the SST model more accurately. The intermittency, plotted on the right-hand side in blue, demonstrates that the transition from laminar to turbulent occurs at around Re = 2000.

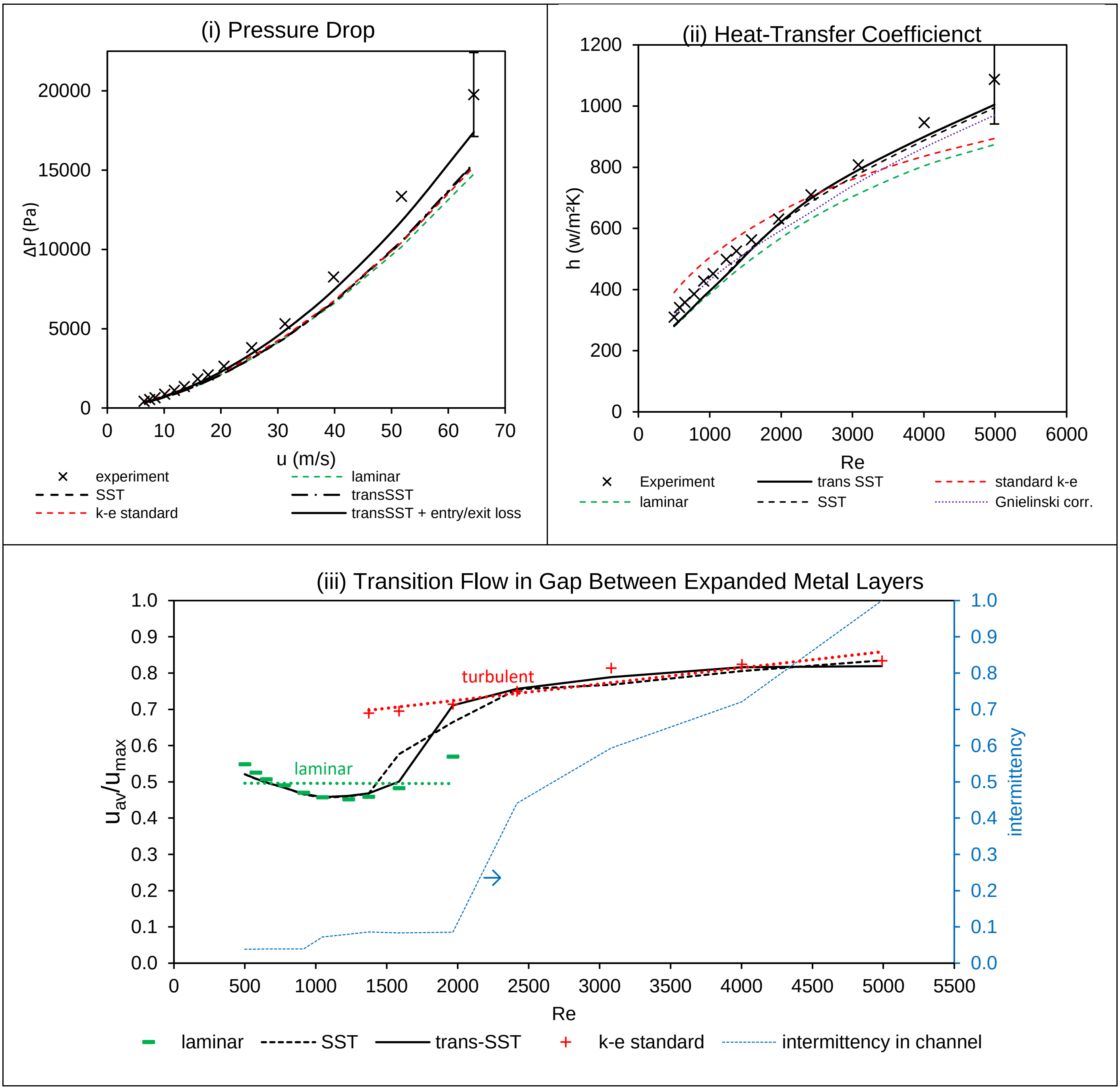

Figure 6: Results of validation. Simulation vs experiment.

Modelling heat transfer in a rotating packed bed

The model was adapted to investigate heat transfer during absorption in an RPB. The absorption process releases heat-of-reaction. This heat was measured experimentally using the apparatus described in Kolawole et al. (3). Energy balance closure was achieved between the temperature rise in the liquid:

$$Q = \dot{m}_L \int_{T_{in}}^{T_{out}} C_p \, dt$$

Against the heat released by the reaction exotherm.

$$Q = \Delta H_r . \dot{m}_{CO2}$$

This shows a typical heating demand of 2,500W for the RPB described in Kolawole et al. (3). The aim was to determine whether an RPB constructed from EM-PMHE, could be capable of removing the heat duty resulting from highlyconcentrated amines. RPBs are uniquely suited to applications involving high-concentration amines and increasing the amine concentration would allow for further size reductions in comparison to conventional technology. However to accomplish this, the process will require heat removal from the absorption process (22).

To model this process, assumptions were made as follows:

1. Heat duty is spread equally over the bed. Experimental measurements of amine temperature at the RPB sump and rotor tip show a small temperature increase in the sump. This implies the amine continues to react and generate heat along the entire length of the RPB bed. RPBs remove mass transfer limitations for the absorption process allowing it to operate close to the kinetic limit: neglecting large temperature changes, this also suggests a relatively uniform heat release in the amine.
2. The packing wetting efficiency, $a_e/a_p \approx 100\%$. Experimental measurements of the wetting efficiency in similar RPBs provide evidence of high wetting efficiencies in RPBs (22).
3. The hold-up is predicted by Yang et al (23).
4. Gas flow conditions are not sensitive to the presence of the liquid on the packing. This is supported by previous experimental work in RPB pressure drop (5).
5. Based on #1 to #4, the amine may be modelled as a thin wall on the packing surfaces, with an energy source term applied to model heat generation inside the amine. The rotor is divided radially into three separate 33mm sections each of constant $\dot{m}_{Gas}$, $\dot{m}_{Liq}$, CSA perpendicular to the flow, ω. The thickness of the film in each section was determined by dividing the surface area by the hold-up liquid volume. The energy source term was defined based on the known duty from experiments, divided by the fraction of the bed volume represented by the CFD geometry.

The results shown below in Figure 7 indicate that an RPB rotor constructed from EM-PMHE would easily remove the heat-of-reaction from the amine to within very close approach temperatures. The model predicts a total temperature rise of 3ºC for the EM-PMHE rotor, compared to +20ºC observed for the conventional rotor during experiments. The model also predicts close approach temperatures, around 2ºC, could be achieved. This means that the absorption could potentially operate at close to isothermal conditions, providing sufficient coolant could be supplied to the EM-PMHE rotor. Figure 7 compares the result from experiments against the simulation result, where the coolant is at 40ºC. It shows that the heat generated in the conventional RPB rotor could be removed with an EM-PMHE-based rotor design.

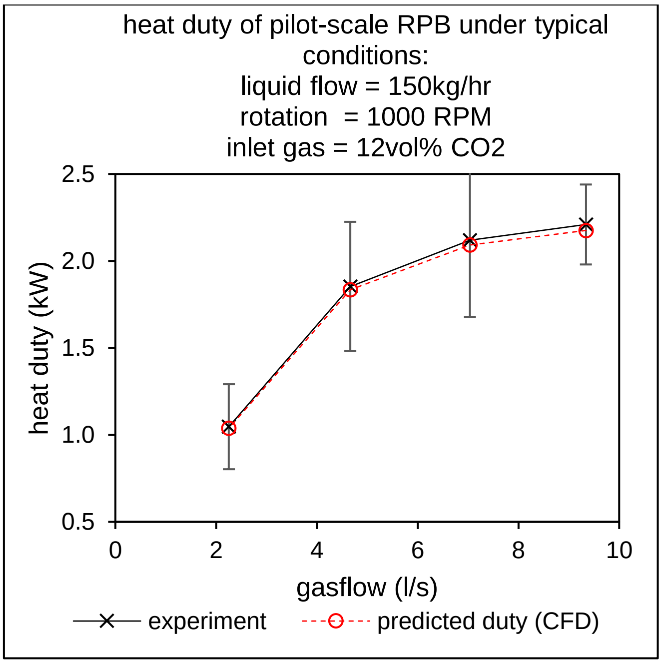

Figure 7: heat generation rate in conventional RPB rotor (experiment) vs. predicted heat removal rate for EM-PMHE rotor (CFD).

Modelling heat transfer in a lean/rich heat exchanger

The EM-PMHE was also assessed for potential application as a lean/rich amine heat exchanger. Results from section 6 were repeated using the material properties of 30wt% MEA. These properties change significantly with temperature and CO_2 loading. To investigate relevant values for the heat transfer coefficient, the range of these variables were taken from the case study (7) (24) and applied to a central composite design (for CFD simulation conditions) based on the sources listed in Table 4. The response was fitted to Reynold's number and Prandlt number using non-linear partial least squares. The resulting fits given below in Equation 4 have a maximum deviation of 6% within the range in Table 4.

Variable:	Range:	Source:
approach temperature ΔT_1	10ºC	(7) (24)
*amine temperature range	40ºC to 120 ºC	(7) (24)
*amine loading range	,α = 0.25 to 0.48 $^{mol\ CO_2}/_{mol\ MEA}$	(7) (24)
*Reynolds number	Re = 250-1250	-
density	1022 to 1077 kg/m^3	(25)
dynamic viscosity	0.575 to 2.256 mPa.s	(26)
heat capacity	,C_p = 3501 to 3717 J/kg-K	(27)
thermal conductivity	0.4837 W/mK	(28)

*Table 4: material properties for lean-rich heat exchanger simulation. *control variables in central composite design.*

Figure 5 compares the CFD model result to the correlation from Equation 4 and the 1D sum-of resistances model described in section 5 above. The sum-of-resistances model gives a comparatively poorer fit with a relative error ca. of 10%-50% likely due to the overprediction of the film heat transfer coefficient from the Gnielinski correlation.

Equation 4: correlation of CFD modelling results for lean/rich heat exchanger simulation.

$$Nu = 0.282\ Re^{0.462}\ Pr^{0.218}$$

$$f = 4.326\ Re^{-0.5}$$

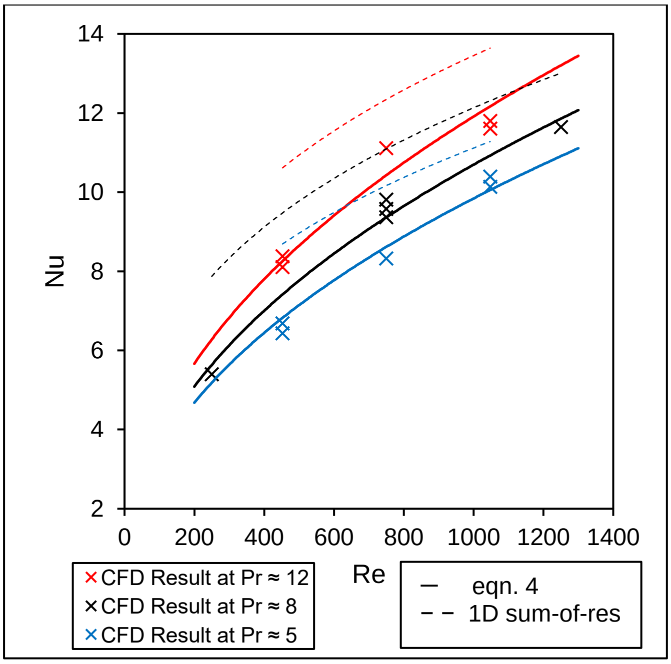

Figure 8: comparison of CFD result to correlation fit from Eqn. 4.

The data from the CFD simulation was used to size a full scale lean/rich heat exchanger, based on established design procedures (29) . For the case study previously discussed (7) (24), lean/rich heat exchange consisted of 22 shell and tube heat exchangers of 963 m^2 heat transfer area per unit – this implies each heat exchanger being roughly 6m x Ø 1.5m based on typical sizes of industrial units. A comparable EM-PMHE was sized at 1.5m x 2.2m x 4m, based on a design pressure drop of 0.7Bar (30). A plant layout comparison based on recommended equipment spacing (31) is given in Figure 9. When compared to the conventional technology, the EM-PMHE gives 10x equipment volume reduction and 24x reduction in estimated plant footprint. While the plant footprint of the shell-and-tube heat exchangers could be reduced through alternative layouts (such as stacked heat exchangers), the sheer scale of these units implies a need for complex structural engineering, pipework layout, control and safety systems. There are clear benefits to replacing these large heat exchangers with a single unit, which would function in a similar manner to any normal heat exchanger. This size estimate is conservative and further size reductions would be possible at higher pressure drops and amine concentrations. The main challenge in the application would be fouling of the EM-PMHE. (in this sizing a fouling resistance of 1/h = 1/6000 W/m^2K was considered for both sides of the exchanger (29)). Fouling in amine processes is chiefly caused by iron sulphide and can be managed through regular flushing of the system (32). It may also be possible to construct dismantlable designs of PMHX suitable for mechanical cleaning.

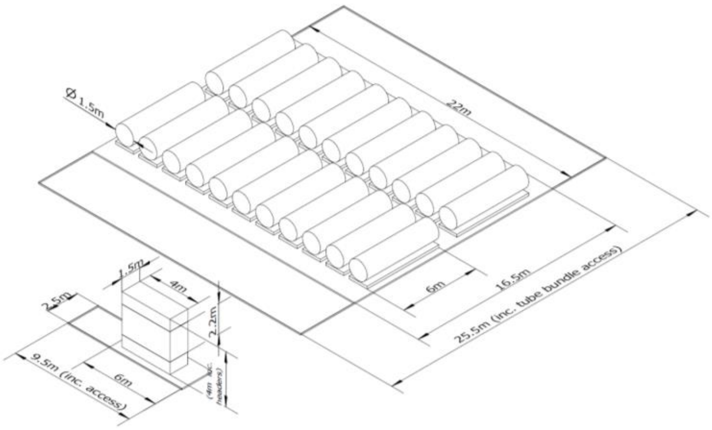

Figure 9 - Plant layout comparison. Shell-and-tube heat exchangers vs. EM-PMHE.

Conclusion

This paper has presented, for the first time, a validated computational fluid dynamics model of an expanded matrix porous metal heat exchanger (EM-PMHE). The model was compared to historical data for EM-PMHE from literature. This demonstrates that it is accurate to within uncertainty from this data for a range of Reynold's numbers across the laminar-turbulent transition. This model was used to test the feasibility of internally cooling a rotating packed bed (RPB), by constructing the packing inside from EM-PMHE material. A simplified approach approximated the amine as a static film on the surface of the packing, based on experimental results from studies on RPBs. This amine film was used to determine whether the heat-of-reaction could be removed by the EM-PMHE. Results indicate a very good predicted performance, with close approach temperatures capable of removing all of the excess heat from the system. EM-PMHE was also considered for the lean/rich heat exchanger in a typical carbon capture process. Comparison between the CFD and the 1D sum-of-resistances model suggests better performance can be obtained from modelling the fluid-flow in three dimensions. Comparison with a conventional carbon capture process indicates significant potential for equipment size reductions in the lean/rich heat exchanger through compact heat exchanger designs. Given that post-combustion carbon capture processes are intended to be retrofitted to existing plants, this reduction in equipment size could be crucially important to their successful implementation particularly in process-industry clusters and other medium-scale carbon capture processes.

Acknowledgements

Authors would like to acknowledge the contributions of the following individuals: Alex Clark, Alex Thornhill.

References

1. *Carbon dioxide absorption and desorption in aqueous monoethanolamine solutions in a rotating packed bed.* **Jassim, MS. Rochelle, G. Eimer, D. Ramshaw, C.** 2007, Industrial & Engineering Chemistry Research 46(9), pp. 2823-2833.

2. **Kolawole, T.** *Intensified post-combustion carbon capture using a pilot-scale rotating packed bed and monoethanolamine solutions.* s.l. : Newcastle University, 2019.

3. *Comparative study of CO2 capture using counter and cross flow configurations in a rotating packed bed absorber using monoethanolamine.* **Kolawole, T, et al.** 2018. 14th Greenhouse Gas Control Technologies Conference Melbourne 21-26 October 2018. pp. 1-8.

4. **Hassan-Beck, MH.** *Process intensification: mass transfer and pressure drop for countercurrent rotating packed beds. .* s.l. : Newcastle University, 1997.

5. *Pressure drop and flooding in rotating packed beds.* **Hendry, J, Lee, J and Attidekou, P.** 2020, Chemical Engineering and Processing - Process Intensification 151, p. 107908.

6. *A mesoscale 3D CFD analysis of the liquid flow in a rotating packed bed .* **Xie, P, et al.** 2019, Chemical Engineering Science 199, pp. 528-545.

7. *Cost estimation of CO2 absorption plants for CO2 mitigation method and assumptions.* **Ali, H, et al.** 2019, International Journal of Greenhouse Gas Control, 88, pp. 10-23.

8. *Intensification of solvent based carbon capture using rotating packed beds.* **Lee, J.** Cranfield : UK Carbon Capture and Storage Research Centre, 2015. UKCCSRC Biannual Meeting Cranfield 21-22 April 2015. .

9. *Investigation of a novel compact heat exchanger surface.* **Hesselgreaves, J.** 1992, UK Energy Efficiency Office Future Practice R&D Profile 29 Best Practice Programme.

10. **Hesselgreaves, J.** *Heat exchangers. 8910241* GB, 1989.

11. *Heat-powered cycles: are process industries missing the boat.* **Reay, D.** 2013, International Journal of Low-Carbon Technologies, 8, pp. 12-18.

12. *Melting of phase change material assisted by expanded metal mesh.* **Mustaffar, A, Harvey, A and Reay, D.** 2015, Applied Thermal Engineering, 90, pp. 1052-1060.

13. **Lide, D.** *CRC handbook of chemistry and physics.* Boca-Raton : CRC, 1992.

14. **Expanded Metal Company.** *Industrial brochure: expanded metal properties.* 2013.

15. **Rohatgi, A.** Webplotdigitizer version 4.4. [Online] 2020. [Cited: July 2021, 01.] https://automeris.io/WebPlotDigitizer.

16. **Hesselgreaves, J.** *Compact heat exchangers: selection design and operation. 2nd ed.* Amsterdam : Elsevier, 2017.

17. **ASME.** Journal of Fluids Engineering Editorial Policy Statement on the Control of Numerical Accuracy. [Online] 2015. [Cited: July 11, 2021.] http://journaltool.asme.org/Content/AuthorResources.cfm (Accessed: 27 July 2015)..

18. **Zigh, G and Solis, J.** *Computational fluid dynamics best practice guidelines for dry cask applications.* Washington : US Nuclear Regulatory Commission, 2013.

19. *Determining heat transfer correlations for transition and turbulent flow in ducts.* **Taler, D and Taler, J.** July 2015, Scientific Letters of Rzeszow University of Technology mechanics.

20. **Green, D and Perry, R.** *Perry's chemical engineers handbook.* 8th. New York : McGraw-Hill, 2007. pp. 788-789.

21. *A correlation-based transition model using local variables`.* **Menter, FR. Langtry, RB. Likki, SR. Suzen, YB. Volker, HS.** 3, 2006, Journal of Turbomachinery, Vol. 128, pp. 413-422.

22. *Study of intercooling for rotating packed bed absorbers in intensified solvent-based CO2 capture process.* **Oko, E. Ramshaw, C. Wang, M.** Applied Energy, Vol. 223, pp. 302-216.

23. *Investigation of effective interfacial area in a rotating packed bed with structured stainless steel wire mesh packing.* **Luo, Y. Lou, J. Chu,G. Zhao,Z. Arowo, M. Chen, J.** 2017, Chemical Engineering Science, Vol. 170, pp. 347-354.

24. *A non-invasive x-ray technique for hold-up in a rotating packed bed.* **Yang, Y. Xiang, Y. Chu, G. Zou, H. Luo, Y. Arowo, M. Chen, J-F.** 2015, Chemical Engineering Science, Vol. 138, pp. 244-255.

25. **Ali, H.** *Techno-economic analysis of CO2 capture concepts (PhD Thesis).* s.l. : University of South-Eastern Norway, 2019.

26. *Density of water monoethanolamine CO2 from 298.15 to 413.15 K and surface tension of water monoethanolamine from 303.15 to 333.15 K.* **Han, J. Jin, J. Eimer, D. Melaeen, M.** 4, 2012, Journal of Chemical Engineering Data, Vol. 57, pp. 1095-1103.

27. *Density and viscosity of monoethanolamine water carbon dioxide from 20 to 80 C.* **Amundsen, G. Oi, L. Eimer, D.** 11, 2009, Journal of Chemical Engineering Data, Vol. 54, pp. 3096-3100.

28. *Heat capacity of aqueous monoethanolamine, diethanolamine, n-methyldiethanolamine, and n-methyldiethanolamine-based blends with carbon dioxide.* **Weiland, R. Dingman, J. Cronin, D.** 5, 1997, Journal of Chemical Engineering Data, Vol. 42, pp. 1004-1006.

29. *Carbon dioxide absorption into monoethanolamine in a continuous film contactor.* **Akanksha, Pant, K. Srivastava, VK.** 2007, Chemical Engineering Journal, Vol. 133, pp. 229-237.

30. **Sinnot, R.** *Coulson and Richardson's Chemical Engineering.* 2nd. Oxford : Pergamon, 1993. Vol. 6.

31. *Cost and emissions reduction in CO2 capture plant dependent on heat exchanger type and different process configurations: optimum temperature approach analysis.* **Aromada, SA. Eldrup, NH. Oi, LE.** 2, 2022, Energies, Vol. 15, p. 425.

32. **Red Bag BV.** BN-DG-C01E Plant Layout - Exchangers. [Online] [Cited: Mar 07, 2022.] www.red-bag.com.

33. *Alkanolamine solution corrosion mechanisms and inhibition from heat stable salts and CO2.* **Veldman, R.** Orlando : s.n., Mar 26, 2000, NACE Corrosion Conference, p. 496.